SUPPLEMENTARY FIGURES AND INFORMATION

Biophysics and Computational Biology

Torsional stress generated by ADF/cofilin on cross-linked actin filaments boosts their severing

Short title: Impact of mechanical stress on cofilin activity

Hugo Wioland, Antoine Jegou*, Guillaume Romet-Lemonne*
Institut Jacques Monod, CNRS, Université Paris-Diderot, Paris, France

*Corresponding authors : Antoine Jegou and Guillaume Romet-Lemonne
Institut Jacques Monod, 15 rue Hélène Brion, 75013 Paris, France
Phone : +33 1 5727 8013
e-mails: antoine.jegou@ijm.fr and romet@ijm.fr

Keywords : cytoskeleton, mechanotransduction, actin dynamics, microfluidics

www.pnas.org/cgi/doi/10.1073/pnas.1812053116116

Supplementary Figures

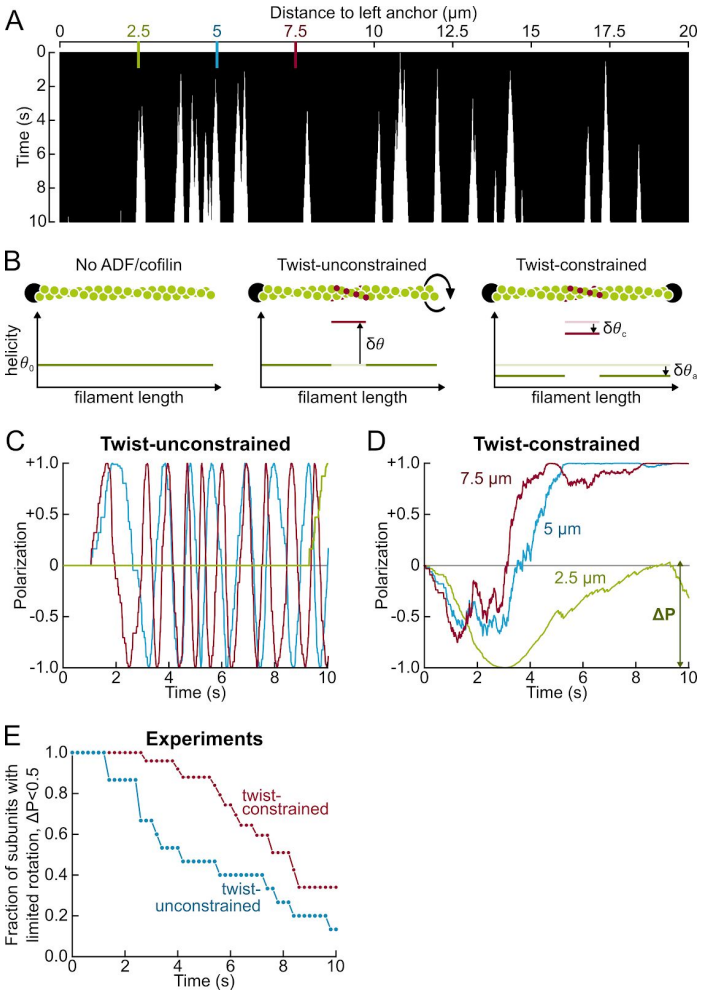

Fig. S1. Actin subunit rotation is hindered by constraining the global twist.

(A) Kymograph of simulated cofilin domains (white) assembling over a 20 μm-long filament. (B) Sketch of local twist deformation. When constrained (right), bare and cofilin-saturated segments are under-twisted, relative to their natural helicity. (C-D) Simulation of three single actin subunit polarization, located 2.5, 5 and 7.5 μm from the left anchor as indicated on A. Polarization is calculated based on cofilin binding shown in A, for twist-unconstrained (C) and twist-constrained (D) filaments. (E) Polarization varies faster in unconstrained filaments (results from experiments). For every actin subunit, the polarization amplitude $\Delta P(t) = max_{t_i \in [0,t]}(P(t_i)) - min_{t_i \in [0,t]}(P(t_i))$ (as shown on D for the green curve).The plot shows the fraction of subunits whose polarization amplitude $\Delta P(t)$ remains lower than 0.5 over time. N=15 for unconstrained and N=25 for constrained filaments. The threshold constant 0.5 was chosen arbitrarily to account for a significant polarization change. In the absence of cofilin, ΔP < 0.5 for all 18 tested subunits over 8s (Fig. 1C).

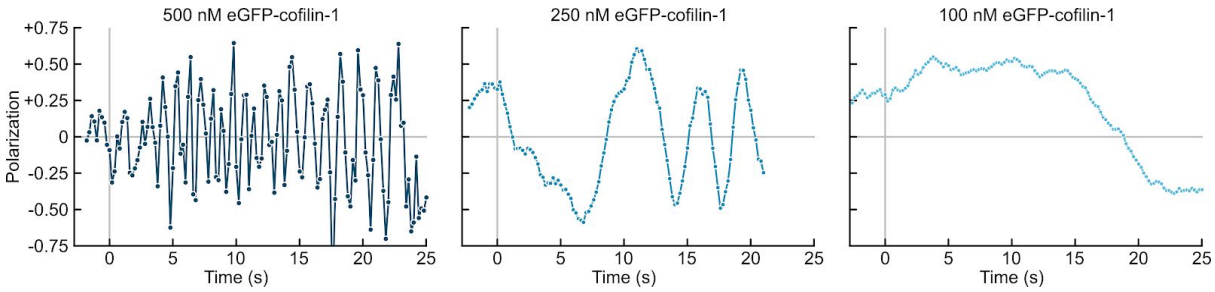

Fig. S2. Polarization oscillation rate increases with cofilin concentration. The oscillation rate increases with cofilin concentration, as expected: it should be proportional to the assembly rate of single cofilin domains times the number of domains assembling at a given time. The former increases with cofilin concentration, and the latter varies over time and globally increases with cofilin concentration at the early times observed here, when the nucleation of new domains is the dominant factor. Unlike in Fig. 1C, filaments were aged for 15 min to allow nearly complete Pi release.

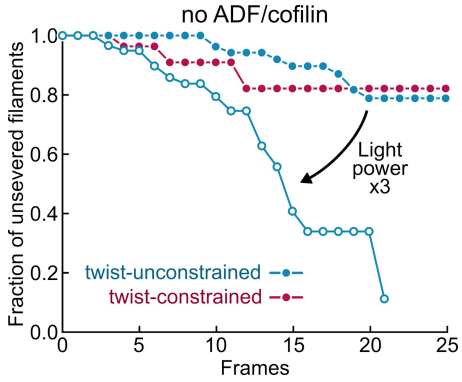

Fig S3: Filaments anchored by one or two ends, barely fragment in the absence of ADF/cofilin.

Experiments were performed as in Fig. 2 except that standard buffer only (no cofilin) was injected from time t=0. Illumination was either as in standard conditions (full symbols), or with a 3-fold higher light intensity (open circles). Survival fractions were calculated with filament lengths matching the average filament length in Fig. 2D, <L> = 6.6 μm (SI methods). Unconstrained filaments, N = 40; constrained, N = 18. Acquisition rate 1 frame / 1.2 s.

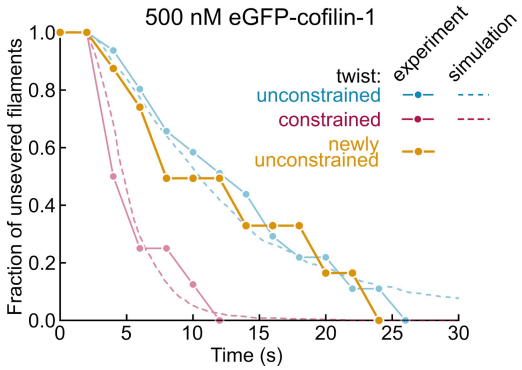

Fig. S4. After severing, double-anchored filaments relax their torque and behave as twist-unconstrained filaments.

Three populations of filaments (N = 16, with the same length distribution) are compared. Blue and red are single- and double- (resp.) anchored filaments that did not sever before the second frame (t = 2s). In orange is a population of filaments that were anchored by both ends at t = 0 and severed before t = 2s. The curve then shows the survival fraction of newly formed actin segments (now anchored by one end only).

Simulations were performed as in Fig. 4, N = 1600, with similar length distribution, excluding severing events occurring before 2s.

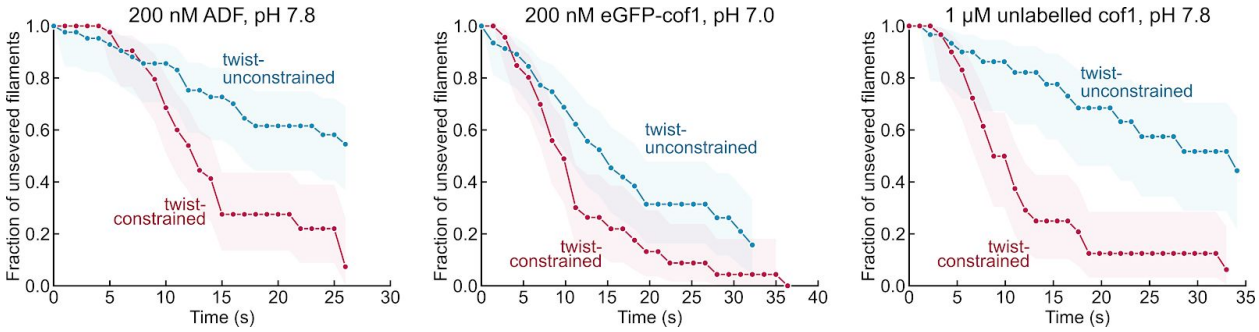

Fig. S5. Faster severing on twist-constrained filaments is observed under different conditions.

Experiments were performed following a similar protocol to Fig. 2: sparsely biotinylated Alexa-568-F-actin was bound to the surface, and a solution containing ADF, eGFP-cofilin-1 or unlabelled cofilin-1 was injected from time t=0 onwards.

Left: 200 nM unlabelled ADF, pH 7.8: N = 42, <L> = 4.1 ± 0.8 µm (std).

Middle: 200 nM eGFP-cofilin-1, pH 7.0: N = 48, <L> = 7.2 ± 3.0 µm (std).

Right: 1 µM unlabelled cofilin-1, pH 7.8: N = 30, <L> = 4.7 ± 0.8 µm (std).

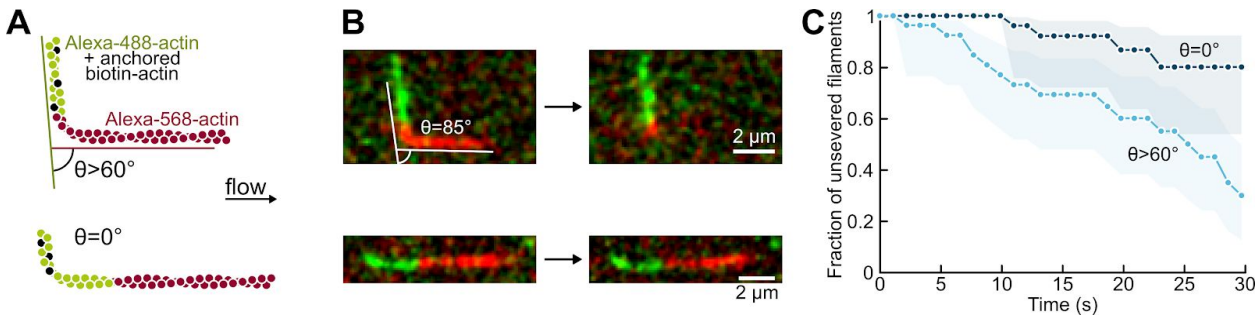

Fig. S6. Bending increases the cofilin-induced severing rate in the absence of phalloidin.
A. We generated in bulk filaments with one segment containing Alexa-488-actin and biotin-actin (which can bind to a neutravidin-decorated surface), and one segment of Alexa-568-actin. Filaments are left to bind the neutravidin-biotin-BSA surface with a random orientation (green). We consider two populations. Top: the filament is bound to the surface up to the Alexa-488/Alexa-568 junction, generating a large angle θ >60°. Bottom: binding occurs >1μm away from the junction, such that segments on both sides of the junction are aligned with the flow, θ=0°. Only severing events taking place near the junction are taken into account.
B. Example of two filaments. The angle θ is defined as the angle between Alexa-488-actin and Alexa-568-actin segments across the junction.
C. Survival fraction of bent (θ >60°) and straight filaments (θ=0°) exposed to cofilin-1. Conditions: 1 μM unlabelled cofilin-1, injected from time t=0. N = 26 (θ=0°) and 27 (θ>60°). <L> = 4.6 ± 1.3 μm, flow gradient: 250/s, the tension applied in the curved region was about 0.2 pN. Shadows represent 95% confidence intervals (SI Methods).
The severing rate, estimated by fitting a simple exponential, is increased 5-fold by bending the filament. The two curves are significantly different, p-value = 0.0049 (logrank test).

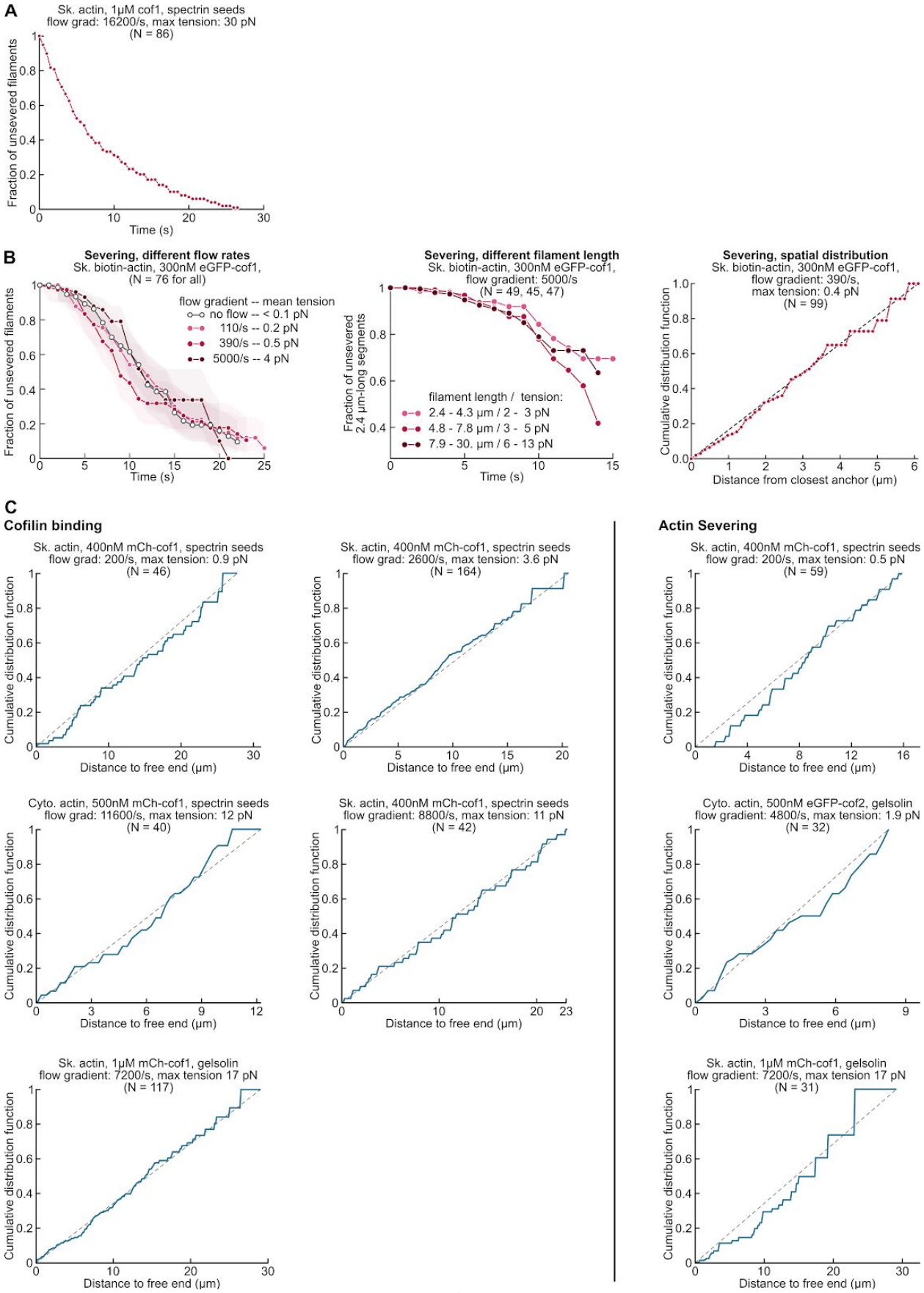
A
Sk. actin, 1μM cof1, spectrin seeds
flow grad: 16200/s, max tension: 30 pN
(N = 86)
Fraction of unsevered filaments
Time (s)
B
Severing, different flow rates
Sk. biotin-actin, 300nM eGFP-cof1,
(N = 76 for all)
flow gradient -- mean tension
no flow -- < 0.1 pN
110/s -- 0.2 pN
390/s -- 0.5 pN
5000/s -- 4 pN
Fraction of unsevered filaments
Time (s)
Severing, different filament length
Sk. biotin-actin, 300nM eGFP-cof1,
flow gradient: 5000/s
(N = 49, 45, 47)
Fraction of unsevered 2.4 μm-long segments
filament length / tension:
2.4 - 4.3 μm / 2 - 3 pN
4.8 - 7.8 μm / 3 - 5 pN
7.9 - 30. μm / 6 - 13 pN
Time (s)
Severing, spatial distribution
Sk. biotin-actin, 300nM eGFP-cof1,
flow gradient: 390/s,
max tension: 0.4 pN
(N = 99)
Cumulative distribution function
Distance from closest anchor (μm)
C
Cofilin binding
Sk. actin, 400nM mCh-cof1, spectrin seeds
flow grad: 200/s, max tension: 0.9 pN
(N = 46)
Cumulative distribution function
Distance to free end (μm)
Sk. actin, 400nM mCh-cof1, spectrin seeds
flow grad: 2600/s, max tension: 3.6 pN
(N = 164)
Cumulative distribution function
Distance to free end (μm)
Cyto. actin, 500nM mCh-cof1, spectrin seeds
flow grad: 11600/s, max tension: 12 pN
(N = 40)
Cumulative distribution function
Distance to free end (μm)
Sk. actin, 400nM mCh-cof1, spectrin seeds
flow gradient: 8800/s, max tension: 11 pN
(N = 42)
Cumulative distribution function
Distance to free end (μm)
Sk. actin, 1μM mCh-cof1, gelsolin
flow gradient: 7200/s, max tension 17 pN
(N = 117)
Cumulative distribution function
Distance to free end (μm)
Actin Severing
Sk. actin, 400nM mCh-cof1, spectrin seeds
flow grad: 200/s, max tension: 0.5 pN
(N = 59)
Cumulative distribution function
Distance to free end (μm)
Cyto. actin, 500nM eGFP-cof2, gelsolin
flow gradient: 4800/s, max tension: 1.9 pN
(N = 32)
Cumulative distribution function
Distance to free end (μm)
Sk. actin, 1μM mCh-cof1, gelsolin
flow gradient: 7200/s, max tension 17 pN
(N = 31)
Cumulative distribution function
Distance to free end (μm)

Fig. S7. Low tension had no effect on cofilin binding and severing regardless of the actin or cofilin isoform, and anchoring method.

A. Surviving fraction showing the severing dynamics of filaments exposed to 1 μM unlabelled cofilin-1 for 2s before switching to standard buffer at time t=0. This graph corresponds to severing distribution shown in Fig. 3 H-I. When observing the position of severing events, two distinct events can occur between two consecutive frames. As the severed fragments are quickly carried away by the flow, only the severing event closer to the anchored point will be observed. To avoid such bias, we acquired movies at a high frame rate: the large majority of severing events correspond to a single event.

B. Severing dynamics of twist-constrained filaments. When actin segments are anchored to the surface by their two ends, the tension generated is nearly uniform. In order to investigate the effect of tension, we compared the severing dynamics of actin segments under different flow rates (left), and of different lengths (middle), as well as the severing spatial distribution (right). Sparsely biotinylated F-actin is anchored to a neutravidin-coated surface, such that actin segments are perpendicular to the flow direction (as presented in Fig. 2B). 300 nM eGFP-cofilin-1 was continuously injected from time t=0 onward.
Left: The experiment was repeated with various flow gradients. Four populations where blindly selected with the same length distributions, $\langle L \rangle = 4.9 \pm 1.2$ μm (N = 76 for each flow rate).
Middle: In a single experiment, filaments were binned into three populations of different lengths. We calculated the survival fraction of 2.4 μm-long segments among these segments (Supp. Methods).
All surviving fraction curves overlap showing that tension had no detectable effect up to 13 pN. Note that at higher tension, the filaments quickly detach from the surface.
Right: We also verified that severing events were homogeneously distributed along double-anchored filaments.

C. Spatial distribution of coflin domains and severing events on filaments anchored by one end only to the surface. Filaments were exposed transiently to 0.4-1 μM cofilin (2 to 5s) before switching to standard buffer at time t=0.
Different conditions were tested. 1) Filaments were either anchored by their pointed- or barbed-end (using spectrin-actin seeds or gelsolin, respectively). 2) Actin isoforms were either α-skeletal or β/γ-cytoplasmic. 3) Different flow gradients were applied, in order to obtain different tension gradients, reaching at maximum 17 pN.
In all cases, the cumulative distribution function follows a linear function, indicating that cofilin domains and severing events are evenly distributed along the tension gradient. Tension has no detectable effect on single-anchored filaments up to 17 pN.

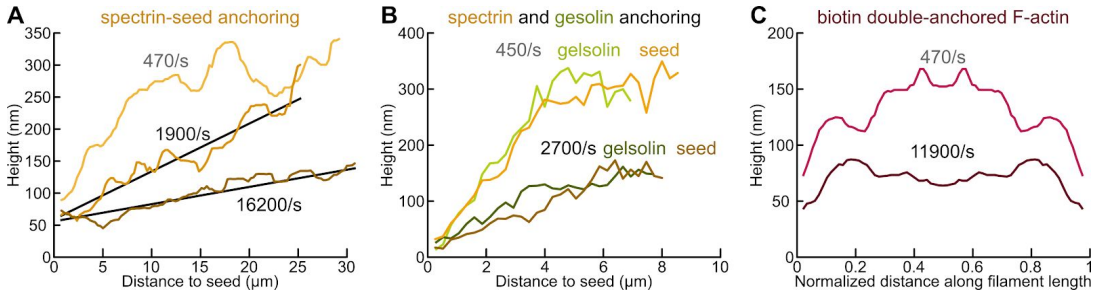

Fig. S8. Filament height profile under different flow gradients and anchoring methods. Filament height were measured from their fluorescence intensity under TIRF illumination (Supp. Info.). Each curve was obtained by averaging the fluorescence of 5 to 10 filaments of similar length, and over 20 to 25 frames for each filament. We used skeletal actin, labelled at 34% with Alexa-488.

With this method, it is difficult to measure the filament height near the anchor (spectrin seed, gelsolin or biotin-neutravidin). We thus ignored the measure in the two first pixels (0.5 μm). In this range (0 to 0.5 μm), the filament height quickly increases from 0 to about 50 nm. This small region was neglected in the tension estimates.

Note that the height profile depends on both the flow gradient but also the filament length. In order to get accurate tension estimates, we measured heights on filaments with similar lengths to that of experiments.

A. Filaments anchored to actin-spectrin seeds appear closer to the surface at strong flow gradients (orange curves). At small flow gradient, <800/s, the filament height reaches a plateau around 250-300 nm from the surface, as described previously (Jegou et al, 2013). At stronger flow rate, >1500/s, the filament height appears to increase linearly. We fitted such curves with linear functions (black lines): $z(x) = z(0) + dz * x$, where $z(0)$ is the filament height near the anchor and dz the height increase along the filament length.

B. Single-anchored filaments have the same height profile regardless of the anchoring method, actin-spectrin seed (orange) or gelsolin (green).

C. Double-anchored filaments. Filaments are sparsely biotinylated and anchored to a neutravidin-coated surface, as in Fig. 2B (Supp. Info.). Here, the filament height was first measured versus the distance to the closest anchor. The distance was then normalized between 0 and 0.5 and mirrored from 0.5 to 1. Typical filament length: 20 μm. After quickly increasing from the anchor, the height seems to reach a plateau. We used the plateau value to estimate the tension over double-anchored filaments (Fig. S7B). Note that filaments appear even closer to the surface than single-anchored filaments.

Supplementary Methods and Information

Biochemistry

Protein purification

Skeletal muscle actin was purified from rabbit muscle acetone powder (Pel-freeze) following the

protocol described in (Wioland et al, 2017) , adapted from the original protocol (Spudich and Watt, 1971).
Cytoplasmic actin was purified from bovine spleen following the procedure detailed in (Schuler et al, 2006).
Spectrin-actin seeds were purified from human erythrocytes as described in described in (Wioland et al, 2017), based on the original protocol by (Casella et al, 1986).
Recombinant human profilin I (Uniprot : P07737) was expressed in E. Coli and purified following the protocol described by (Gieselmann et al, 1995).
Mouse cofilin-1 (Uniprot : P18760), as well as fluorescently tagged eGFP-cofilin-1 and mCherry-cofilin-1 were purified as described previously in (Kremneva et al, 2014).
Human ADF (hADF, Uniprot : P60981) and human gelsolin (Uniprot : P06396) were purified as described previously in (Wioland et al, 2017).

Protein labelling
Actin was fluorescently labeled on accessible surface lysines of F-actin, using Alexa-488 or Alexa-594 succinimidyl ester (Life Technologies). To minimize effects from the fluorophore we used a labeling fraction of 10 to 15 %. Cofilin-1 was fused with mCherry or eGFP at their N-terminus (Kremneva et al, 2014). We used either unlabelled or 100 % labeled cofilins as specified. We have previously verified in vitro that labeled cofilins remain fully functional (Wioland et al. 2017)
Gelsolin was biotinylated as follow: 400 µL 5 µM gelsolin was dialysed overnight at 4°C against 500 mL PBS pH 7.5, 1 mM EGTA, 0.01 % NaN_3. Sulfo-NHS-LC-LC-biotin (EZ Link, ThermoFisher) was then added at 20-fold molar excess and left at room temperature for 1h. Biotin-gelsolin was then dialysed against 500 mL 20 mM Tris pH 7.5, 150 mM NaCl, 0.01 % NaN_3, 1 mM EGTA (twice 2h, 4°C) and stored at -80°C.

Buffers
We performed most experiments in F-buffer: 5 mM Tris HCl pH 7.8, 50 mM KCl, 1 mM $MgCl_2$, 0.2 mM EGTA, 0.2 mM ATP, 10 mM DTT and 1 mM DABCO. DTT and DABCO limit light-induced artifacts. F-buffer was supplemented with 0.4 mM $CaCl_2$ when injecting gelsolin (Ca-F-buffer).

Microfluidics and Microscopy
Microfluidic chamber
Protein solutions were injected into a Poly Dimethyl Siloxane (PDMS, Sylgard) chamber, 20 µm in height, 800 µm in width and ~1 cm in length. Chambers were mounted on glass coverslips previously cleaned in ultrasound baths of 1M NaOH followed by ethanol. PDMS chambers and glass coverslips were UV-treated to allow them to bind tightly to each other. We used cross-shaped channels with 3 inlets (Figure 2A). We control the pressure in the reservoir and measured the flow rate in each channel using microfluidic devices MFCS and Flow Units (Fluigent).
T-shaped open chambers (used in Fig. 5 only) were assembled using double-sided tape, and coverslips which were previously cleaned, passivated with 5 % biotin-BSA for 15 minutes, rinsed in water, and dried. Solutions were flowed in by capillarity, and blotted out using Whatmann paper. After introduction of F-actin, the short channel (the base of the “T”) was sealed with nail polish.

F-actin polymerization and anchoring

Different approaches were used to anchor actin filaments to the surface :

- **Spectrin-actin seeds** : injected at 2 to 20 pM and left to bind non-specifically to the surface for 1 to 2 minutes. The surface was then passivated with either bovine serum albumin (BSA, 5%, > 10 min) or PLL-PEG (SuSos, 1 mg/mL, >1h). Filaments are then grown using a solution of, typically, 0.8 µM G-actin, 0.8 µM profilin. Filaments are finally aged for > 15 min with G-actin at critical concentration (0.1 µM), to ensure that the actin is in > 99.9% ADP-state. This method generates actin filaments anchored solely by their pointed-end to the surface.
- **Gelsolin**: the chamber was first passivated with 0.2 % biotin-BSA (5 min) and 5% BSA (10 min). 3 µg/mL neutravidin was then injected for 5 min before rinsing with Ca-F-buffer. The chamber was then incubated with ~5 pM biotin-gelsolin in Ca-F-buffer for ~5 min. F-actin was prepolymerized, typically, at 4 µM for >1h. Filaments were finally injected into the chamber, gelsolin would bind to their side, sever the filament and stay bound to the newly generated barbed-end. Filaments do not interact with the surface otherwise.
- **Biotin-actin**: The chamber was first incubated with 1 mg/mL PLL-PEG and 0.01 mg/mL PEG-biotin for > 1h. The surface was further passivated with 5% BSA (10 min) before incubating with 10 µg/mL neutravidin for 5 min. F-actin, containing ~2 % biotin-actin, was prepolymerized and injected perpendicularly to the long axis of the chamber (Fig. 2A). Filaments bind to the neutravidin-coated surface by a few points along their length. ADF/cofilin is finally injected in the direction along the main axis, such that actin segments bound to the surface by one end only align with the flow, and segments bound by the two ends, form arcs, aligned perpendicularly to the flow direction. When ADF/cofilin severs the latter segments, the newly formed two halves align with the flow, thus revealing the exact position of the anchoring points (Fig. 2B). This method then generates, in a single field of view, tens of actin segments anchored by either one or two ends (unconstrained or constrained twist, respectively), whose behavior can be directly compared.
- **Anchored phalloidin-stabilized actin segments**: the chamber was prepared following the previous method. Unlabelled biotin-actin filaments were prepolymerized (10 µM, 1h) and stabilized with an equimolar concentration of rhodamine-phalloidin (left to incubate 5 min). The suspension was vigorously pipetted to generates smaller actin fragments, diluted down to 0.1 µM, injected into the chamber, and left to bind the surface in the absence of flow such that stabilized actin filaments bind the surface with random orientation. Filaments were then elongated from these segments with 0.3 µM Alexa-488-G-actin for > 15 min, generating filaments with two straight regions and a highly curved segment at the junction between the anchored and stabilized segment (red) and the free-floating segment (green, Fig 3A-B).

Polarization measurement

In order to measure single actin monomer orientation, filaments were polymerized with 0.4 % Alexa-568-actin, following either the spectrin-actin seed or biotin-actin method. The sample was imaged with epi-fluorescence and the emitted light was split into two channels (Optosplit II ByPass, Cairn Research) polarized at +45° and – 45° with respect to the filament main axis.

Acquisition

The microfluidic setup was placed on a Nikon TiE or TE2000 inverted microscope, equipped with a 60x oil-immersion objective and an optional additional 1.5x magnification. We either used TIRF, HiLo or epifluorescence depending on the background fluorophore concentration in solution. The TiE microscope was controlled by Metamorph, illuminated in TIRF or epifluoresence by 100 mW tunable lasers (ILAS2, Roper Scientific), and images were acquired by an Evolve EMCCD camera (Photometrics). The TE2000 microscope was controlled by micromanager (Edelstein et al, 2014), illuminated with a 120W Xcite lamp (Lumen dynamics) and images were acquired by an sCMOS Orca-Flash2.8 camera (Hamamatsu).

Force calibration

Fluid flow in microfluidics chambers exerts a drag force on filaments. We estimated this force following our previously published method (Jegou et al, 2013). Briefly, the force generated on a short segment of length *dl* is $df = dl.v.\mu$, where v is the local fluid velocity and μ the friction coefficient $\mu = 0.0006\ pN.s/\mu m^2$ (Jegou et al, 2013). The tension of the filament at a distance l from the free end is then given by $T(l) = \mu \int_0^l v(dl).dl$.

Inside the chamber, the fluid velocity follows a parabolic profile along the vertical axis, $v(z) = 6z(h-z)R/(h^3 w)$, where z is the height of the filament, R is the global flow rate (as measured on Fluigent Flow Meter), h and w the height and width of the chamber. Since $z \ll h$, we approximate the parabolic profile as linear near the surface: $v(z) = z.6R/(h^2 w)$. We indicate in the figure captions of each experiment the flow gradient, $6R/(h^2 w)$ (with units s^{-1}).

To estimate the height of the filaments, we measured their fluorescence intensity I under TIRF illumination: $I(z) = I(0)\ exp(-z/d)$, where $I(0)$ is the filament intensity at z=0 and d the TIRF penetration depth. We measured $I(0)$ using biotinylated and fluorescent filament anchored to a surface along their length with neutravidin.

The penetration depth was estimated from the build-in software (ILAS2, Roper Scientific) and by measuring the intensity of fluorescent beads in the same flow profile (Jegou *et al.*, 2013). Both number were consistent, 185 nm and 190 nm respectively and decided to use the former.

We measured the filament height profile under different flow profiles and anchoring methods.

- Spectrin-seed-anchored filaments: as reported earlier, under a low flow gradient (< 1000/s), filament height increases quickly to reach a plateau around 250-300 nm (Fig. S8A). However, when the flow is further increased, the filament height linearly increases from the seed to the free end. We measured this height for filament lengths similar to those used in experiments. For example, at 16200/s (Fig 3 E-I and Fig. S8A), the filament height is well fitted by $z(x) = 60\ nm + 0.0027\,x$, where x is the distance to the seed, in nm.
- We compared this height with other anchoring methods. Anchoring with gelsolin at the barbed-end instead of spectrin-seeds did not change the filament height profile (Fig. S8B). However, biotin-actin filaments anchored by their two ends appear closer to the surface (Fig. S8C).

Data analysis

Polarization (Fig. 1C, 1B, 1G, Supp. Fig. S1)

The orientation of single fluorophores was followed by 1) identifying the fluorophore in both polarization channels, 2) measuring the mean fluorescence intensity, I_{+45} and I_{-45}, in a 5x5

pixel ROI containing the fluorophore, from which the intensity of the neighboring background was subtracted, 3) calculating the fluorophore polarization as $P = \frac{I_{+45} - I_{-45}}{I_{+45} + I_{-45}}$.
The binding of cofilin was measured as the total increase in fluorescence (minus the local background) from the spectrin-actin seed to the actin fluorophore of interest. The fluorescence of a single cofilin was estimated by measuring the intensity along a saturated filament, divided by the total number of cofilin molecules bound. The estimated number of cofilin bound is finally calculated as the increase of fluorescence divided by the fluorescence of a single cofilin monomer.
Images were typically acquired every 200ms when imaging actin only (Fig 1C-D) and every 2 s when imaging both actin and cofilin (Fig. 1G). In order to reduce noise, cofilin fluorescence was smoothed over 5 data points (Fig 1C-D).

Cofilin binding to twist-constrained and -unconstrained filaments (Fig. 2C)
The density of cofilin was calculated as:

$$D = A \frac{I^{fluo}_{cof} - I^{bgd}_{cof}}{I^{fluo}_{actin} - I^{bgd}_{actin}},$$

where I_{cof} (resp. I_{act}) is the intensity of cofilin (resp. actin channel), I^{fluo} the mean fluorescence along the filament, I^{bgd} the mean fluorescence in the surrounding background, and 'A' a constant normalization factor to ensure that the density *D* of saturated filaments is 1. The density was measured and averaged over ten individual filaments for each condition. For twist-constrained filaments, the density was monitored before and after severing.

Calculating the survival fraction / fraction of unsevered filaments
During the course of an experiment, biotin-actin filaments might detach from the surface, either through the release of the biotin-neutravidin link, or the unsticking of biotin-PLL-PEG. This is particularly visible at high flow rate (i.e. high filament tension). Likewise, severing events often occur at the anchor or seed due to the sharp bent of the filament. All these events do not correspond to regular severing event and are taken into account as 'lost' filaments. We use the Kaplan-Meier method to estimate the survival fraction f_{surv} and confidence interval (Kaplan 1958). The survival fraction was calculated as follow:

$$f_{surv\,(t=0)} = 1,$$
$$f_{surv\,(t)} = f_{surv\,(t-1)} * \frac{N_{surv\,(t)}}{N_{surv\,(t)} + N_{sev\,(t)}},$$

where $N_{surv\,(t)}$ is the number of filament still intact at frame t, and $N_{sev\,(t)}$ the number of filaments that severed between frames t-1 and t. To distinguish severing events from anchoring detachment, severing events must occur at least 2 pixels away from the anchor and thus some actin fragment must still be visible at the anchoring site after severing. Note that if a filament detaches on a frame t, it will still be counted as an intact filament (N_{surv}) on all previous frames.
When comparing filaments of different lengths (Fig. S3 and Fig. S7B), longer filaments tend to sever faster since they hold more cofilin domains. In order to normalize by the length, we adjusted the formula of f_{surv} as follow:

$$f_{surv\,(t)} = f_{surv\,(t-1)} \cdot \left(1 - \frac{n_{sev\,(t)} \cdot dl}{L(t-1)}\right),$$

Where $n_{sev}(t)$ is the number of severing events at time t, dl the length of the smallest filament (2.6 µm on Fig. S7B) and $L(t-1)$ the total length of filaments at time t-1, that have not been lost on frame t.

The confidence interval (shaded area on Fig. 2, 3, 4) was calculated using the exponential Greenwood formula (Kalbfleisch 1980):

$$exp(-exp(c_{+(t)})) < f_{surv(t)} < exp(-exp(c_{-(t)}))$$

where

$$c_{\pm(t)} = log(-log(f_{surv(t)})) \pm z\sqrt{V}$$

$$V = \frac{1}{(log(f_{surv(t)}))^2} * \sum_{t_i<t} \frac{N_{sev(t)}}{N_{surv(t)} * (N_{surv(t)} + N_{sev(t)})}$$

And $z = -1.96$ for 95% confidence interval.

Cumulative distribution of cofilin domains and severing events position (Fig. 3)

Since biotin-actin filaments bind to the surface randomly, the length of unconstrained and constrained segments can largely vary. A simple solution would be to use only filaments of similar length. Alternatively, we use all filaments but weighting every event depending on their position and filament length distribution.

Moreover, at high flow rate, the tension gradient is not linear (because the filament height continuously increases as a function of distance to the anchoring point). As a consequence, the length of the filament segment corresponding to a given range of tension is not constant. When plotting the cumulative distribution versus tension, this effect has to be taken into account by renormalizing by the length of filament for each given tension.

We perform two types of measurements:

- **Multiple events on a single filament: cofilin domain distribution.** The number of domains appearing at a given tension *T* (or distance to one end) is proportional to the number of filaments and length of F-actin at that tension. The weight is then

$$w_{(T)} = 1 / \sum_{i,j} \delta(T_i^j = T),$$

  where T_i^j is the tension at the pixel j on the filament *i*, *T* is the tension at the position of the given domain, and $\delta(b) = 1$ if the condition *b* is true, 0 otherwise.
- **Single event per filament: severing events distribution.** When an event can only occur once on a filament, the probability to appear at a given position is inversely proportional to the length (or tension range) of that filament. The weight then becomes

$$w_{(T)} = N_k / \sum_{i,j} \delta(T_i^j = T),$$

where N_k is the number of pixels on the filament *k* on which the event occured.

The weights are further normalized such that their sum equals to 1. The cumulative distribution function is then calculated as the sum of the weights of all events j (severing, cofilin domains, etc) happening at a lower tension than T,

$$f_{cum.\,distri.}(T) = \sum_{j:T_j<T} w_j.$$

Binning (Fig 3 G,I) is calculated similarly by dividing the number of events by the number of pixels available in a tension range. In the case of domain distribution we assume that, at maximum, we can detect one domain every 3 pixels because of the diffraction limit.

Statistical significance

P-values were calculated with different methods depending on the measure:

- Domain density. We used a Fisher's exact test. Each sample is a different tension range (or bin). We assume N_{site} binding site (i.e. measure) as the total number of pixels in a given tension range divided by 3. N_{domain}, the number of domains, correspond to a positive outcome and $N_{site} - N_{domain}$ as a negative. We used the function *fisher_exact* from the Python package *scipy.stats*.
- Severing probability. Since we only recorded the first severing event over each filament, the number of severing over two different tension ranges are correlated. To compare two tension bins *B1* and *B2*, we only counted the number of events in each bin $N_{sev}{}^{1}$ and $N_{sev}{}^{2}$. We then used a one-sample binomial test using the experimental ratio $N_{sev}{}^{1}/(N_{sev}{}^{1} + N_{sev}{}^{2})$, compared with the null-hypothesis $N_{pix}{}^{1}/(N_{pix}{}^{1} + N_{pix}{}^{2})$, where $N_{pix}{}^{i}$ is the number of pixels in the bin *Bi*. We used the function *binom_test* from the Python package *scipy.stats*.
- Survival fraction. When calculating surviving fractions with the Kaplan-Meier method, we compared entire curves using the logrank test. We used the function *logrank_test* from the Python package *lifelines.statistics*.

Softwares

All measurements (length, distance, fluorescence intensity, severing timing, etc) were performed manually on ImageJ. All data were stored in Microsoft Excel and analyzed using Python (software Pyzo). Simulations were also performed using Python.

Computations of forces on double-anchored filaments

Constrained twist: nearly uniform tension

When filaments are anchored by both ends instead, the viscous drag also generates a tension along the filament, but its computation is more complex. As in single anchored filaments, each actin segment 'feels' a viscous force *F* proportional to the local fluid velocity $\nabla v\, h$, the segment length l, the friction coefficient λ and, weakly, the segment orientation φ:

$$F = \lambda\, \nabla v\, h\, l\, (2\, cos\, (\varphi)^{2} + sin\, (\varphi)\,).$$

The factor 2 reflects the fact that the friction generated by a flow perpendicular to a thin rigid cylinder is approximately twice that of a flow along the same cylinder (Hancock 1953, Hinch 1991).

In our experiments, filaments are anchored orthogonally to the channel's main axis, and are only slightly curved. The angle $\varphi \ll \pi/2$ and we can simplify F as:

$$F = 2\, \lambda\, \nabla v\, h\, l.$$

Estimating the tension of the filament then boils down to the classical problem of the catenary, where the friction coefficient $2\,\lambda$ corresponds to the density, and $\nabla v\, h$ to the acceleration of gravity g. The problem can then easily be solved by balancing forces, friction (in the flow direction) and tension (tangential to the filament): $F + T_0 + T = 0$ (, where T is the tension and the anchoring point, T_0 the tension at the midpoint (i.e. where $\varphi = 0$), and F the friction force between these two points.

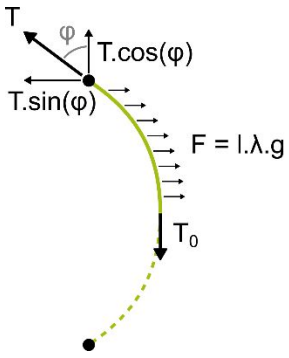

Projecting the previous equation along the flow direction gives:

$$T.sin(\varphi) = 2\,\lambda\,\nabla v\,h\,L/2,$$

where L is the length of the filament.
Likewise, projecting in the perpendicular direction to the flow:

$$T.cos\,(\varphi)\; = T_0.$$

The tension T is then larger than the friction F by a factor $1/(2sin\,(\varphi)\,)$. Estimated over 30 filaments, $\varphi = 17°$ (std dev. = 4°). Then,

$$T \approx 3.4\,F\; = 3.4\,\lambda\,\nabla v\,h\,L,$$

$$T_0 \approx 3.3\,F\; = 3.3\,\lambda\,\nabla v\,h\,L.$$

The factor 3.4 (respectively, 3.3) goes down to 2.8 (respectively, 2.6) when taking $\varphi = 17 + 4°$ (mean + std dev.), and 4.5 (respectively, 4.4) with $\varphi = 17 - 4°$ (mean - std dev.).
This result also shows that the tension on double-anchored filaments is 3.4-fold larger than the maximum tension reached by single-anchored filaments.
Interestingly, T_0 is barely smaller than T. We thus assume the tension to be uniform along the filament.

Torque generated by ADF/cofilin binding

When binding to twist-constrained filaments, ADF/cofilin locally increases the natural right-handed helicity. But since the global twist must remain constant, this will deform the filament, put it in an under-twisted configuration and generate a torque Γ.
In order to estimate this deformation and the torque generated, we consider the total number of turns θ (angle) to go from the first to the last actin subunit of one actin strand (right handed helicity). On a twist-unconstrained filament, θ depends on the number of cofilin molecules bound. We assume that the binding of every cofilin molecule, on either strand, increases θ by a constant angle $\delta\theta$. The global additional rotation is then

$$\Delta\theta\; = \theta(v) - \theta(0) = \;L\,/\,dl\;.\;\nu\;.\;\delta\theta,$$

where L is the length of the filament, $dl = 2.7\;nm$ the effective subunit length (L divided by the total number of actin monomers), and ν the density of cofilin on the filament ($0 \le \nu \le 1$).
Cryo-EM structures indicate that the right-handed half-pitch (i.e. crossover distance) goes from 36.5 nm for a bare filament ($\nu = 0$), to 27.0 nm for a cofilin-saturated filament ($\nu = 1$, McGough et al, 1997). Every cofilin molecule then adds $\delta\theta \approx 4.7°$ to the total rotation θ.

When filaments are twist-constrained, the overall rotation θ cannot increase and we assume that the local helicity at a bare (respectively, cofilin-decorated) actin subunit will decrease by an angle $\delta\theta_a$ (respectively, $\delta\theta_c$). In order to keep the global rotation constant, deformations should follow

$$\nu\;.\;(\delta\theta - \delta\theta_c) - \;(1 - \nu).\;\delta\theta_a = 0.$$

Also, at equilibrium, the torque is uniform throughout the filament:

$$\Gamma = C_a \,.\, \delta\theta_a/dl \;=\; C_c \,.\, \delta\theta_c/dl,$$

where C_a (respectively, C_c) is the torsional rigidity of a bare (respectively, cofilin-decorated) actin subunits.
Rewriting the two previous equations yields:

$$\Gamma = [\, \nu \, \tfrac{\delta\theta}{dl} \,]. \, [\tfrac{C_a \,.\, C_c}{\nu \,.\, C_a + (1-\nu).\, C_c}]$$

The second half of the expression reflects an effective mean torsional rigidity over the filament. Importantly, cofilin-decorated filaments have been observed to be more flexible than bare filaments ($C_c < C_a$). We used values from (Prochniewicz et al, 2005):

- $C_a \;=\; 2.3 \,.\, 10^3 \; pN.nm^2/rad$,
- $C_c \;=\; 0.13 \,.\, 10^3 \; pN.nm^2/rad$.

Overall, the filaments becomes more flexible as the ADF/cofilin density increases, leading to a faster increase of Γ at low ν, when the filament is stiffer, than at high ν, when the filament is more flexible. The resulting curve is plotted in Fig. 4B.
The maximum force moment $\Gamma_{(\nu=1)} = 3.9 \; pN.nm$.

Theory

Energy of cofilin binding

Experimentally, cofilin binds globally at a similar rate on twist free and constrained filaments. Yet binding to constrained filaments means deforming the filament, which will cost energy, opposing cofilin binding. Therein, we compare the energy gained from binding (biochemical interactions between cofilin and actin molecules) with that necessary to deform the filament.
1. Binding energy
Based on cofilin affinity, Cao *et al.* estimated the free energy change (Cao et al, 2006)

$$\Delta G^{\circ'}_{T} = \; -13.8 \; kJ.mol^{-1} \;=\; -5.5 \; k_B T = \; -22.6 \; pN.nm,$$

for a single isolated cofilin molecule, and the energy associated with cooperativity

$$\Delta G^{\circ'}_{coop} = \; -7 \; kJ.mol^{-1} \;=\; -2.8 \; k_B T = \; -11.5 \; pN.nm.$$

All together, the addition of a cofilin molecule to a domain releases an energy more than $8 \; k_B T$.
2. Twisting energy
The energy associated with twisting follows a quadratic law,

$$E_{twist} = \tfrac{1}{2} \tfrac{C}{L} \theta^2,$$

where C is the torsion rigidity, L the length over which the object is deformed and θ the angle of deformation (in radians). For a constrained filaments with a density v of cofilin bound, the energy then becomes

$$E_{twist} = \tfrac{1}{2} (\tfrac{C_a}{dl} \theta_a^2 \tfrac{L}{dl} (1 - v) + \; \tfrac{C_c}{dl} \theta_c^2 \tfrac{L}{dl} v),$$

Replacing θ_a and θ_c gives

$$E_{twist} = \tfrac{1}{2} \tfrac{L \, \delta\theta^2}{dl^2} \tfrac{C_a C_c}{v C_a + (1-v) C_c} v^2.$$

Deriving the equation then gives the extra energy needed to add a cofilin molecule

$$\Delta E_{twist} = \delta\theta (\tfrac{v \, \delta\theta}{dl} \tfrac{C_a C_c}{v C_a + (1-v) C_c}) (1 - \tfrac{1}{2} \tfrac{v(C_a - C_c)}{v C_a + (1-v) C_c}),$$

where the first parenthesis corresponds to the torque, and in the second parenthesis, the first term corresponds to the extra energy from twisting and the second is associated with the decrease in the average torsion rigidity.
The energy per cofilin molecule increases with density and reaches a maximum at saturation

$$\Delta E_{twist}(v = 1) = 0.04\ k_B T = 0.17\ pN.nm.$$

For consistency, we used values of C_a and C_c (Prochniewicz et al, 2005) and $\Delta G^{\circ'}_T$ (Cao et al, 2006) both calculated by the group of Enrique M. De La Cruz.
Overall the energy associated with twisting is two orders of magnitude lower than that of binding which explains why no significant difference was observed between cofilin binding on twist-unconstrained and twist-constrained filaments.

Simulations

Binding

To simplify, filaments are modelled as 1D. One ADF/cofilin molecule can bind between two adjacent actin subunit. *In vitro* and *in vivo*, the establishment of a new domain is a complex and poorly understood process involving the transient binding of ADF/cofilin and cooperative effects. To simplify, we assume that new domains appear as a single ADF/cofilin binds a bare region. However, to account for cooperativity, the nucleation rate k_{new} is chosen quadratic with the concentration:

$$k_{new} = 5.6\ .\ 10^{-5}\ .\ (\frac{[cof]}{0.2})^2\ /s\ ,$$

where $[cof]$ is the concentration of cofilin in µM, and $5.6\ .10^{-5}/s$ is the nucleation rate we measured at 0.2 µM eGFP-cof1 (Wioland 2017). There is no fitted parameter but the choice of the model (quadratic) is arbitrary.

For the elongation of ADF/cofilin domains, we assume that subunits can be added at the very border of domains, with the same rate toward the pointed or barbed end:

$$k_{on}^{eff} = k_{on}\ .\ [cof] - k_{off} = 13\ .\ [cof] - 0.7\ /s\ ,$$

where k_{on} and k_{off} were measured by fitting at different concentration of eGFP-cof1 (Wioland 2017). Again, we are not fitting any parameter. To simplify, we do not simulate the unbinding of subunits (except indirectly through the value of k_{on}^{eff}), especially since at ADF/cofilin concentrations used in experiments, the dynamic is dominated by elongation. Likewise, the unbinding from within a domains is extremely slow and is neglected here (Wioland 2017).

Severing

Experiments have shown that ADF/cofilin induces severing at the border of domains, with a bias towards the PE. To simplify, we assume severing only occurs at borders towards the pointed-end. In the absence of torque (filaments anchored by one end only), the severing rate per border is assumed constant, $k_{sev} = k_{sev}^0$.
When a torque Γ builds up (constrained filaments), the severing rate is modulated by a modified Bell model,

$$k_{sev} = k_{sev}^0.exp\ (\alpha\ \frac{\Gamma}{k_B T})$$

where $k_B T$ is the product of the Boltzmann constant and the temperature, $k_B T = 4.1\ pN.nm$. k_{sev}^0 takes the same value as for single-anchored filaments. α, a constant, is the only fitted parameter.

Fitting

The only two fitted parameters are k_{sev}^0 and α. We chose arbitrarily to fit them with measurements at 1 µM eGFP-cofilin-1. Without changing the parameters, this fitting is then compared with experiments at 250 and 500 nM eGFP-cofilin-1 (Fig. 4).

k_{sev}^0 is first fitted on the fraction of unsevered single-anchored filaments (twist-free). This yielded:

$$k_{sev}^0 = 2.5 \,.\, 10^{-2} \, /s \,.$$

Keeping the same value for ksev, α was then fitted over the fraction of unsevered double-anchored filaments (fixed twist), yielding:

$$\alpha = 5 \,.$$

To fit these parameters, simulations are performed with a population 50-fold larger than that of the experiment (N = 48), but with exactly the same filament length distribution. Parameters are adjusted manually to minimize the sum of the square of the difference between experiments and simulations.

Supplementary Information References

- Cao W, Goodarzi JP, De La Cruz EM (2006). Energetics and kinetics of cooperative cofilin–actin filament interactions. Journal of molecular biology 361(*2):257*-267.
- Casella JF, Maack DJ, Lin S (1986) Purification and initial characterization of a protein from skeletal muscle that caps the barbed ends of actin filaments. J Biol Chem 261:10915–21.
- Edelstein A, Tsuchida M, Amodaj N, Pinkard H, Vale R, and Stuurman N (2014), Advanced methods of microscope control using µManager software. Journal of Biological Methods 2014 1(2):e11
- Gieselmann R, Kwiatkowski DJ, Janmey PA, Witke W (1995) Distinct biochemical characteristics of the two human profilin isoforms. Eur J Biochem 229:621–628.
- Hancock GJ (1953) The self-propulsion of microscopic organisms through liquids. Proc. R. Soc. Lond. A 217(1128):96-121.
- Hinch EJ (1991) Perturbation methods. Cambridge university press.
- Jégou A, Carlier MF, Romet-Lemonne G (2013) Formin mDia1 senses and generates mechanical forces on actin filaments. Nature communications 4:1883
- Kalbfleisch JD, Prentice RL (1980) The statistical analysis of failure time data. John Wiley & Sons, New York.
- Kaplan EL, Meier P (1958) Nonparametric Estimation from Incomplete Observations. J Am Stat Assoc 53:457.
- Kremneva E et al. (2014) Cofilin-2 controls actin filament length in muscle sarcomeres. Dev Cell 31:215–226.

- McGough A, Pope B, Chiu W, Weeds A (1997) Cofilin changes the twist of F-actin: implications for actin filament dynamics and cellular function. The Journal of cell biology 138(4):771-781.
- Prochniewicz E, Janson N, Thomas DD, De La Cruz EM (2005) Cofilin increases the torsional flexibility and dynamics of actin filaments. Journal of molecular biology 353(5):990-1000.
- Schuler H, Karlsson R, Lindberg U (2006) Purification of non-muscle actin Third edit. Elsevier Inc.
- Spudich JA, Watt S (1971) The regulation of rabbit skeletal muscle contraction. I. Biochemical studies of the interaction of the tropomyosin-troponin complex with actin and the proteolytic fragments of myosin. J Biol Chem 246: 4866–71.
- Wioland H et al. (2017). ADF/Cofilin accelerates actin dynamics by severing filaments and promoting their depolymerization at both ends. Current Biology 27(13):1956-1967.